Boundary layer growth and advection of heat over snow and soil patches: Modelling and parametrization

Essery, Richard Lawrence Howard; Granger, Raoul; Pomeroy, John W.

Published in:
Hydrological Processes

DOI:
10.1002/hyp.6122

Publication date:
2006

Citation for published version (APA):
Essery, R. L. H., Granger, R., & Pomeroy, J. W. (2006). Boundary layer growth and advection of heat over snow and soil patches: Modelling and parametrization. *Hydrological Processes*, *20*(4), 953-967. https://doi.org/10.1002/hyp.6122

Boundary layer growth and advection of heat over snow and soil patches: Modelling and parametrization

Richard Essery[1], Raoul Granger[2] and John Pomeroy[3]

[1]*Institute of Geography and Earth Sciences, University of Wales Aberystwyth, UK*

[2]*Environment Canada, National Water Research Institute, Canada*

[3]*Department of Geography, University of Saskatchewan, Saskatoon, Canada*

Short title: Modelling advection over patchy snow

Corresponding author:

Richard Essery

Institute of Geography and Earth Sciences

University of Wales Aberystwyth

Aberystwyth SY23 3DB

UK

Email: rie@aber.ac.uk

Tel : +44 (0)1970 622784

Fax : +44 (0)1970 622659

Abstract:

Melting snow is generally patchy; upward sensible heat fluxes from patches of snow-free ground warm the air and contribute energy for snowmelt. A simple model is presented for advection of heat over partial snowcovers and compared with measurements of temperature profiles over snow and snow-free ground. Approximations for flux and temperature profiles in the internal boundary layers over snow patches are used to develop parametrizations for local and average surface fluxes into the snow. In comparison with results from the advection model for regular patterns of alternating snow patches and snow-free ground, a tile model is found to give a good parametrization for average heat fluxes over the whole surface but does not match the local fluxes into snow and snow-free ground separately; an extended tile model that gives better results is developed from the flux profile parametrization. For complex snowcover patterns with a fractal distribution of patch sizes, average fluxes are found to be close to those obtained for a regular pattern with an effective patch size linearly related to the average patch size of the complex pattern.

INTRODUCTION

The initial melt of a homogeneous snowcover can be driven by radiation or large-scale advection of warm air, but snow inevitably becomes patchy as it melts. Snow-free ground has a much lower albedo than snow, and is not limited to a maximum temperature of 0°C, so it can become substantially warmer than the surrounding snow, and upward fluxes of sensible heat from the snow-free ground warm the air. As this warmed air flows over a snow patch, downward heat fluxes cool the air and warm the snow; heat is thus advected from snow-free ground to snow and provides an additional source of energy for melt. An internal

boundary layer (IBL) in which air temperatures and heat fluxes differ from those at the upwind edge of the snow patch develops and grows in depth with downwind distance. Vertical temperature profiles and IBL growth rates have been measured over snow patches by Takahara and Higuchi (1985) and Granger et al. (2005).

Advection of heat to snow patches has been investigated previously using high-resolution boundary-layer models that solve the Navier-Stokes equations with the Boussinesq approximation and some flux closure (Weisman 1977, Liston 1995, Essery 1997). Such models are computationally expensive and prone to numerical instabilities, limiting their application to simple snowcover geometries and narrow parameter ranges. As an alternative, a highly simplified advection model is presented here. The model is first evaluated in comparison with measurements of temperature profiles and IBL growth rates from Granger et al. (2005).

Simple methods for calculating the advection of heat to patchy snowcovers are required for practical applications. From measurements of temperatures over a patchy tundra snowcover, Marsh and Pomeroy (1996) developed an empirical index for the efficiency with which heat fluxes from snow-free ground contribute to fluxes into snow; this has been used to represent advection in the VIC hydrological model (Cherkauer and Lettenmaier 2003) and the snowmelt model of Pohl and Marsh (2005). Granger et al. (2002) suggested a method based on integration of the horizontal advection of heat through the depth of the IBL at the upwind and downwind edges of a snow patch to find the net advection.

For large-scale atmospheric and hydrological models, efficient parametrizations are required to calculate average surface fluxes on the catchment or grid scales on which these models are applied. Patterns of fractional snowcover are not explicitly represented on subgrid scales. Gridbox-average surface fluxes have to be calculated using measured air temperatures or gridbox-average air temperatures on the lowest model level, which is typically 10 to 20 m above the

surface in a global atmospheric model. Although the standard assumption of a constant-flux layer fails for heterogeneous surfaces, the same equations used to calculate fluxes over homogeneous surfaces can be used with effective parameters for heterogeneous surfaces if there exists a height range above the 'blending height' at which horizontal variations in temperature fall below some threshold that is still sufficiently close to the surface that the average vertical flux is close to the average surface flux (Mahrt 2000). A more direct method for calculating fluxes over heterogeneous surfaces is to gather distinct surface types within a gridbox into homogeneous 'tiles' and calculate fluxes separately over each tile (Avissar and Pielke 1989). Using this method to calculate local surface fluxes in addition to average fluxes relies on the assumption that flux perturbations, which extend higher than temperature perturbations, will still be close to their surface values at the temperature blending height (Wood and Mason 1991). For surfaces with small horizontal variations in heat flux, tile models have been found to give good estimates of the local fluxes produced by boundary-layer models (Wood and Mason 1991, Essery 1997). Clearly, this will not be the case for a surface with regions of both upwards and downwards flux, as often occurs for partial snowcover. If there is a downwards flux into the snow but the average flux over an area of partial snowcover is upwards, there will be a temperature maximum at some height above the snow. The heat flux thus changes direction from downwards at the surface to upwards above the temperature maximum, and the local flux at the blending height is far from its surface value. In comparison with simulations for partial snowcover, Liston (1995) found that a tile model could give a good estimate of average heat fluxes, but Essery (1997) found that the separate fluxes over snow and snow-free ground were not well represented. For an atmospheric model, only gridbox-average fluxes between the surface and the atmosphere are required as boundary conditions. If fluxes from distinct surface types within the

surface are not accurately represented, however, evolving errors in surface state variables such as soil moisture or fractional snowcover will lead to evolving errors in average fluxes.

In this paper, the surface flux parametrization suggested by Granger et al. (2002), which is based on integration of the energy conservation equation, is developed and supplemented by a second parametrization based on an assumed form for the flux profile within an IBL and integration of the flux-gradient relationship; both parametrizations are evaluated in comparison with results from the advection model for isolated snow patches. For regular patterns of alternating snow patches and snow-free patches, a tile model is again found to give a good simulation of average fluxes but a poor simulation of local fluxes in comparison with the advection model. An extended tile model, based on the second integral parametrization, is found to give better results. Finally, the advection model is used to simulate fluxes over more realistic complex snowcover patterns, and the resulting flux distributions are related to results from simulations with regular snowcover patterns.

MODEL DESCRIPTION

A crucial simplification in the model used here is that horizontal adjustments in windspeed over heterogeneous surfaces are neglected, so the model is not suitable for application to large contrasts in surface roughness or heterogeneity on length scales large enough for the generation of mesoscale circulations. The windspeed is assumed to follow a logarithmic profile

$$U(z) = \frac{u_*}{\kappa} \ln\left(\frac{z + z_0}{z_0}\right), \tag{1}$$

where u_* is a velocity scale, z is the height above the surface, z_0 is the surface roughness length and κ is the von Kármán constant. Energy conservation then

gives the downwind evolution of potential temperature T with distance x as

$$U\frac{\partial T}{\partial x} = \frac{1}{\rho c_p}\frac{\partial H}{\partial z}, \tag{2}$$

where ρ and c_p are the density and heat capacity of air and H is the vertical heat flux, taken to be positive when directed downwards. The heat flux is related to vertical temperature gradients through

$$H = \rho c_p \frac{\kappa u_*(z+z_0)}{\phi(z/L)}\frac{\partial T}{\partial z}. \tag{3}$$

This first-order closure is used for efficiency, although higher-order schemes may be more appropriate for non-equilibrium conditions near changes in surface characteristics (Rao et al. 1974, Garratt 1992). The influence of atmospheric stability on eddy diffusivities is represented by the stability function

$$\phi(z/L) = \begin{cases} [1-16(z+z_0)/L]^{-1/2} & L<0 \text{ (unstable)} \\ 1+5(z+z_0)/L & L>0 \text{ (stable)} \end{cases} \tag{4}$$

where

$$L = \frac{\rho c_p T u_*^3}{\kappa g H} \tag{5}$$

is the Monin-Obukhov length and g is the gravitational acceleration.

Surface flux H_0 is obtained by integrating Equation (3) over z from 0 to the height z_1 of the lowest model level, assuming a constant flux. This gives

$$H_0 = \rho c_p \kappa u_*(T_1 - T_0)\left[\ln\left(\frac{z_1+z_0}{z_0}\right) - \psi\left(\frac{z_1}{L}\right)\right]^{-1} \tag{6}$$

where T_0 is the surface temperature, T_1 is the temperature at z_1 and

$$\psi = \begin{cases} 2\ln\left[\frac{1+(1-16(z_1+z_0)/L)^{1/2}}{1+(1-16z_0/L)^{1/2}}\right] & L<0 \\ -5z_1/L & L>0 \end{cases} \tag{7}$$

An implicit numerical scheme is used to solve Equation (2) on a regular grid with a 10 cm spacing in the horizontal and 2 cm in the vertical, extending up to

a fixed-temperature boundary condition at a height of 4 m. Greater numerical efficiency could be achieved by using a stretched vertical grid.

ADVECTION OVER AN ISOLATED SNOW PATCH

Temperature profiles and IBL growth

Granger et al. (2005) describe a system for making simultaneous measurements of temperature profiles above snow and snow-free ground. The system consists of two masts, each with a vertical array of fine-wire thermocouples. One mast is placed on snow-free ground and the other is placed on a snow patch. Figure 1 shows temperature profiles measured above bare soil with an estimated roughness length of 2 mm (crosses) and 2.5 m downwind from the edge of a snow patch (diamonds); the windspeed at a height of 2 m was 6.3 ms^{-1}.

If there is a sufficient fetch of snow-free ground for a constant-flux layer to have developed to some arbitrary height, inverting Equation (6) gives a temperature profile

$$T_u(z) = T_g + \frac{H_u}{\rho c_p \kappa u_*} \left[\ln\left(\frac{z+z_0}{z_0}\right) - \psi\left(\frac{z}{L}\right) \right] \tag{8}$$

for temperature T_g and heat flux H_u on the snow-free surface. Fitting Equation (8), as shown by the dashed line on Figure 1, gives T_g = 11.3°C and H_u = -85 Wm^{-2}. It should be noted, however, that the surface temperature measured with an IR thermometer was 8.9°C; such a discrepancy could result from heating of the air by vegetation elements, spatial variations in surface temperature due to variations in the wetness of the soil or the mismatch between radiative and aerodynamic surface temperatures. This is not considered further, as surface temperatures are not explicitly modelled here.

Equation (8) is used as an inflow boundary condition for simulations of advection over isolated snow patches. As air flows over snow at temperature $T_0 < T_g$, a downward heat flux into the snow cools the air. Assuming that the snow surface

temperature was 0°C, the solid line on Figure 1 shows that taking a snow surface roughness length of 0.2 mm in the model gives a good match to the measured profile.

The difference between the profiles near the ground in Figure 1 shows that there was an IBL over the snow patch. One possible definition for the depth of the developing IBL is the height z_b such that, given some ϵ,

$$|T(x,z) - T_u(z)| < \epsilon \tag{9}$$

for $z \geq z_b$. Figure 2 shows IBL depths calculated from temperature profiles measured at various distances from the upwind edges of snow patches in fields of different roughness (Granger et al. 2005). The lines on Figure 2 were obtained from modelled temperature profiles with $\epsilon = 0.05$.

Many theoretical and experimental studies (reviewed by Brutsaert 1982) have found that IBL growth downwind of a change in surface characteristics can be approximated by a power law

$$z_b(x) \approx cx^b. \tag{10}$$

The use of logarithmic axes in Figure 2 emphasises that power laws give good fits to both the measured and modelled IBL depths. Granger et al. (2005) present results from seven sets of experiments grouped into three classes according to the roughness of the snow-free ground, showing that the rate of IBL growth increases with increasing upwind roughness and increasing temperature contrasts. The simple model used here, however, allows investigation of a far wider range of surface and atmospheric conditions.

Some features of IBL growth can be determined by a scaling analysis of Equations (1), (2) and (3). Ignoring the influences of atmospheric stability by setting $\phi = 1$ and introducing the dimensionless coordinates $Z = (z+z_0)/z_0$ and $\chi = x/z_0$

gives

$$\frac{\partial T}{\partial \chi} = \frac{\kappa^2}{\ln Z} \frac{\partial}{\partial Z} \left(Z \frac{\partial T}{\partial Z} \right), \tag{11}$$

which is independent of windspeed and surface roughness. IBL growth in the dimensionless coordinates is assumed to follow

$$Z = c' \chi^{b'}, \tag{12}$$

with b' and c' independent of windspeed and surface roughness, giving

$$z_b \approx c' z_0^{1-b'} x^{b'}. \tag{13}$$

Comparing with Equation (10), this suggests that b and c should be independent of windspeed, b should be independent of surface roughness, and c should scale as z_0^{1-b}; assuming that $b < 1$, this gives an increasing IBL growth rate for increasing roughness.

Figure 3 shows how b and c obtained from simulations vary with surface roughness z_0, 2 m windspeed U_2, surface temperature difference $T_g - T_0$ and upwind stability measured by H_u; as each parameter is varied in turn, the others are held at constant values of $z_0 = 2$ mm, $U_2 = 4$ ms^{-1}, $T_g - T_0 = 5$°C and $H_u = -50$ Wm^{-2}. Figure 3(a) also shows results derived from measured profiles by Granger et al. (2005) for three roughness classes. Results in Figures 3 (a) and (b) broadly confirm the conclusions of the scaling arguments above. For variations in upwind surface roughness, c increases approximately as $z_0^{0.3}$, but b shows a weak decrease with increasing roughness in both simulations and observations. The coefficients are nearly independent of windspeed, except at low windspeeds for which the IBL depth becomes undefined; with no advection, there is no IBL growth. In calm conditions, thermal gradients can induce "snow breeze" circulations (Segal et al. 1991, Taylor et al. 1998), but this behaviour is not reproduced by the model. Figures 3 (c) and (d) include results for both positive and negative values of

$T_g - T_0$ and H_u to cover the cases of isolated snow patches and isolated snow-free patches. The coefficients are approximately linear functions of H_u, with b and c both decreasing as the upwind temperature profile is made progressively more unstable. For fixed H_u, there is no IBL growth when there is no temperature difference, but c increases with increasing magnitudes of the temperature difference. Both b and c take slightly larger values for the unstable case of cold air being advected over a warm surface ($T_g - T_0 < 0$) than the reverse.

Because the diffusion coefficient in Equation (3) increases with height, flux perturbations extend higher above the surface than temperature perturbations (Philip 1996). Although flux profiles are not available from the observations of Granger et al. (2005), IBL heights can be determined from simulated flux profiles through the condition

$$|H(x, z_b) - H_u| < \epsilon |H_0 - H_u|, \tag{14}$$

so that the difference between upwind and downwind fluxes is less than a fraction ϵ of the surface flux difference for heights greater than z_b. This gives IBL heights that are greater than those determined from temperature profiles but can still be approximated by a power law. Flux measurements over heterogeneous surfaces either have to be made above this height to obtain representative area-average fluxes, or a footprint analysis has to be used to interpret the results (Schmid 1997).

Parametrization of surface fluxes

A boundary-layer integration method for parametrizing the advected heat flux into a snow patch was suggested by Granger et al. (2002). Integrating Equation (2) over x from 0 to patch length X and over z from 0 to IBL height z_b gives

$$\int_0^X [H_0(x) - H(x, z_b)] dx = \rho c_p \int_0^{z_b} U(z)[T_u(z) - T(X, z)] dz. \tag{15}$$

Here, $H_0(x)$ and $H(x, z_b)$ are local fluxes at the surface and the top of the IBL; $T_u(z)$ and $T(X, z)$ are temperature profiles above the upwind and downwind edges of the patch. If z_b is taken to be the flux IBL height, rather than the temperature IBL height used by Granger et al. (2002), Equation (15) gives

$$\langle H_0 \rangle = H_u + \frac{\Delta S}{X}, \tag{16}$$

where $\langle H_0 \rangle$ is the average heat flux into the snow and ΔS is the difference in horizontal transport of heat between the upwind and downwind edges of the patch due to cooling of the air.

To evaluate the right-hand side of Equation (15), the temperature profile at the downwind edge of the snow patch has to be known. Simulated flux and temperature profiles at the downwind edge of a 10 m snow patch are shown by solid lines on Figures 4 (a) and (b), and crosses on Figure 4(b) show the equilibrium temperature profile for a constant-flux layer. The temperature and heat flux profiles are only in equilibrium with the snow in a shallow layer near the surface. Above this equilibrium layer, the temperature profile adjusts towards the upwind profile at the top of the IBL and cannot be described by a constant-flux profile. Instead, suppose that the flux profile can be approximated by

$$H(z) = H_u + (H_0 - H_u)\left(1 + \frac{az}{z_b}\right)\exp\left(-\frac{az}{z_b}\right). \tag{17}$$

This profile is chosen to have the boundary conditions $H(0) = H_0$, $H'(0) = 0$ and $H(z) \to H_u$ as $z \to \infty$. Choosing a as the solution of

$$(1 + a)e^{-a} = \epsilon, \tag{18}$$

the profile also satisfies the IBL condition Equation (14); for $\epsilon = 0.05$, this gives $a = 4.74$. Integrating Eq. (3) using Eq. (17) gives the temperature profile as

$$T(z) = T_0 - \frac{1}{\rho c_p \kappa u_*}\int_0^z \frac{\phi}{z + z_0}\left[H_u + (H_0 - H_u)\left(1 + \frac{az}{z_b}\right)\exp\left(-\frac{az}{z_b}\right)\right]dz. \tag{19}$$

Stability has only a small influence for a shallow IBL and moderate stability; simplifying Equation (19) by setting ϕ=1 gives

$$T(z) = T_0 + \frac{H_u}{\rho c_p \kappa u_*} \ln\left(\frac{z + z_0}{z_0}\right) + \frac{(H_0 - H_u)}{\rho c_p \kappa u_*} \mathcal{E}(z), \tag{20}$$

where

$$\mathcal{E}(z) = \int_0^z \left(1 + \frac{az}{z_b}\right) \exp\left(-\frac{az}{z_b}\right) \frac{dz}{z + z_0}. \tag{21}$$

Equation (21) can be expressed in terms of exponential integrals, for which approximations are available (Abramowitz and Stegun 1976), or evaluated numerically. H_0 is found by evaluating Equation (20) for $z = z_b$ and matching $T(z_b)$ to the known temperature $T_b = T_u(z_b)$ at the top of the IBL, to give

$$H_0(x) = H_u - \frac{1}{\mathcal{E}(z_b)} \left[H_u \ln\left(\frac{z_b + z_0}{z_0}\right) + \rho c_p \kappa u_* (T_b - T_0) \right]. \tag{22}$$

This gives the local flux into the snow surface at a distance x from the upwind edge such that the IBL height is z_b. Using a power law approximation for z_b, Equation (22) is compared with simulated fluxes in Figure 4 (c). To find the average heat flux into a snow patch, Equation (22) can be integrated over x or Equation (20) can be used in a numerical integration of Equation (15). Figure 4 (d) compares Equation (15) with average simulated fluxes for patches of varying size. Parametrization errors in comparison with simulated average and local fluxes are greatest for small patches or close to the patch edge, decreasing to less than 10% for x and X greater than 0.5 m.

ADVECTION OVER PARTIAL SNOWCOVER

In the preceding section, it was assumed that the boundary layer was fully developed upwind of the snow patch and had a temperature profile in equilibrium with the surface heat flux. Although the early or late melt stages of a snowcover may be characterized by isolated snow-free patches surrounded by snow or

isolated late-lying snow patches, this will not generally be the case for a partial snowcover with alternating patches of snow and snow-free ground. Advection over partial snowcover is considered below, first for regular snowcover patterns and then for complex patterns. The advection model is now run with periodic horizontal boundary conditions rather than an inflow boundary condition

Regular snowcover patterns

Previous modelling studies (Liston 1995, Essery 1997) have considered regular snowcover patterns, with snow patches of length X covering a fraction f of the surface. Figure 5 shows simulated surface fluxes for $f = 0.5$ and $X = 5$ m (dashed line) or 10 m (solid line). Heat fluxes into the snow are greatest at the upwind edges of the snow patches and decline as the air is cooled travelling over the patches. Because there are smaller upwind snow-free fetches, the maximum heat flux into the snow is smaller for smaller length scales: 155 Wm^{-2} for $X = 5$ m and 161 Wm^{-2} for $X = 10$ m in Figure 5. Because there are more snow-free to snow transitions, however, the average flux into the snow is greater: 62 Wm^{-2} for $X = 5$ m and 53 Wm^{-2} for $X = 10$ m.

As found by Weisman (1977) for simulations of heat fluxes into isolated snow patches, the flux at a distance x from the upwind edge of each snow patch in a regular pattern can be approximated by a power law

$$H_0(x) = dx^{-n}. \tag{23}$$

Parameters obtained by fitting Equation (23) to simulations with 10 m snow patches, varying snow-free fetches and two different roughness lengths are shown in Figure 6. For a regular snowcover pattern, the snow-free fetch is related to the snow patch size and the snowcover fraction through

$$X_{\mathrm{bare}} = \left(\frac{1-f}{f}\right) X. \tag{24}$$

The coefficient d increases rapidly with increasing fetch and is a linear function of z_0 while the exponent n remains within a fairly narrow range and is less sensitive to z_0; both d and n approach constant values for large fetches.

Marsh and Pomeroy (1996) introduced the concept of the efficiency with which heat flux H_{bare} from snow-free ground contributes to the flux H_{snow} into snow, such that

$$H_{\text{snow}} = H_{\text{snow}}^{\infty} + \left(\frac{1-f}{f}\right) F_s H_{\text{bare}}, \tag{25}$$

where H_{snow}^{∞} is the heat flux at the downwind edge of a large snow patch with negligible advection and F_s is the advection efficiency; this is expected to approach 1 for near-complete snowcover and 0 for very small snowcover fractions. Advection efficiencies for fluxes calculated using bulk formulae and temperature measurements over snow and snow-free areas at a tundra site in 1993 (Marsh et al. 1997) and 1996 (Neumann and Marsh 1998) are shown in Figure 7; an approximately exponential decrease in advection efficiency with increasing snow-free area is observed. Figure 7 also shows advection efficiencies calculated from simulations with 20 m and 200 m domain sizes; heat is more efficiently advected for snowcovers with smaller patch sizes. The observations show a sharper decrease in efficiency with decreasing snowcover than the simulations do, but there is a great deal of scatter in the observations. It should also be noted that air temperatures at the measurement height may themselves be influenced by advection, reducing the accuracy of fluxes calculate from bulk formulae.

Tile models are often used to calculate average fluxes over heterogeneous surfaces, calculating separate fluxes for distinct surface types using the air temperature on a reference level at or above the blending height. For snow patches with temperature T_{snow} and snow-free patches with temperature T_{bare}, a tile model based on Equation (6) would calculate average surface heat fluxes for snow and

snow-free ground as

$$H_{\text{snow}} = \rho c_p \kappa u_* (T_{\text{ref}} - T_{\text{snow}}) \left[\ln\left(\frac{z_{\text{ref}} + z_0}{z_0}\right) - \psi\left(\frac{z_{\text{ref}}}{L_{\text{snow}}}\right) \right]^{-1} \tag{26}$$

and

$$H_{\text{bare}} = \rho c_p \kappa u_* (T_{\text{ref}} - T_{\text{bare}}) \left[\ln\left(\frac{z_{\text{ref}} + z_0}{z_0}\right) - \psi\left(\frac{z_{\text{ref}}}{L_{\text{bare}}}\right) \right]^{-1}, \tag{27}$$

where z_{ref} is set to the temperature blending height and T_{ref} is the temperature at that height. The domain-average surface flux is then given by

$$\langle H_0 \rangle = f H_{\text{snow}} + (1 - f) H_{\text{bare}}. \tag{28}$$

Tile model predictions are compared with results from simulations with varying snow patch sizes and fractions in Figures 8 (a) and (b). As found previously, the tile model closely matches domain-average fluxes but gives poor estimates of local fluxes over snow and snow-free ground separately. Fitting power laws to average fluxes from the simulations gives $H_{\text{snow}} \approx 87 X^{-0.21}$ and $H_{\text{bare}} \approx -106 X^{-0.12}$ to very good approximations.

Although Equation (15) still applies in principal to average surface fluxes over patches, the temperature profiles at both the upwind and downwind edges of a patch are now unknown *a priori*, complicating its application. Equation (17), however, might provide a parametrization for *average* flux profiles above distinct surface types. Extending Equation (10) to partial snowcover, the height at which the fractional difference between average fluxes falls below some threshold can be approximated by a function of the form

$$z_b \approx c \left(\frac{1 - f}{f}\right)^{1/2} X^b, \tag{29}$$

and the temperature at that height can be estimated as

$$T_b = \langle T_0 \rangle + \frac{\langle H_0 \rangle}{\rho c_p \kappa u_*} \left[\ln\left(\frac{z_b + z_0}{z_0}\right) - \psi\left(\frac{z_b}{L}\right) \right], \tag{30}$$

with $\langle H_0 \rangle$ supplied by the tile model; $\langle T_0 \rangle$ is the domain-average surface temperature. Adapting Equation (22), average fluxes over the snow-covered and snow-free fractions are then given by

$$H_{\text{snow}} = \langle H_0 \rangle - \frac{1}{\mathcal{E}(z_b)} \left[\langle H_0 \rangle \ln \left(\frac{z_b + z_0}{z_0} \right) + \rho c_p \kappa u_* (T_b - T_{\text{snow}}) \right] \tag{31}$$

and

$$H_{\text{bare}} = \langle H_0 \rangle - \frac{1}{\mathcal{E}(z_b)} \left[\langle H_0 \rangle \ln \left(\frac{z_b + z_0}{z_0} \right) + \rho c_p \kappa u_* (T_b - T_{\text{bare}}) \right]. \tag{32}$$

Dashed lines on Figures 8 (a) and (b) show that this extended tile model gives much closer matches to the simulated fluxes than the tile model did.

Complex snowcover patterns

Partial snowcovers do not, of course, consist of regularly spaced snow patches. Instead, they have been observed to have fractal characteristics. Analysing aerial photographs, Shook et al. (1993) found the number of snow patches of area A or greater to follow a power-law relationship

$$N(A) \sim A^{-D_k/2} \tag{33}$$

with D_k between 1.2 and 1.8. Similarly, Granger et al. (2002) found a relationship

$$X \sim A^{D_h/2} \tag{34}$$

between area and length scale X for snow patches, with $D_h = 1.25$. The number of patches with length X or greater thus scales as

$$N(X) \sim X^{-h} \tag{35}$$

with $h = D_k/D_h \approx 1$.

Shook and Gray (1997) described a method for generating synthetic two-dimensional snowcovers with realistic characteristics. Because only patterns of snowcover along transects are required here, the simpler method of generating

patch lengths by sampling random numbers with a distribution given by Equation (35) is used. Thirty simulations were performed in 200 m domains with 50% snowcover, giving a total of 5200 snow patches. Figure 9 (a) shows the average fluxes into snow patches of different sizes in these simulations; vertical bars extend to one standard deviation on either side of the averages. In terms of advection efficiency, these simulations would plot very close to the upper (short length scale) curve in Figure 7.

Some features of the average fluxes into snow patches of varying sizes in a complex pattern can be deduced from results for regular patterns if it is assumed that local fluxes can be approximated by Equation (23) with an exponent that is independent of patch size. The average flux into patches of a particular size will then be a power-law function of the patch length with the same exponent as for a regular pattern; the solid line on Figure 9(a) is a power law with an exponent of -0.22, very close to the value of -0.21 obtained for regular patterns with the same roughness and stability in the preceding section. The variance of the patch fluxes will be a decreasing function of patch length because the flux is less sensitive to upwind conditions for larger patches; in fact, a logarithmic function of patch length (dashed lines) gives a good fit to standard deviations.

The temperature of the air at the upwind edge of a snow patch is determined by additions and subtractions of heat as the air passes over many upwind snow-free and snow patches, so it might be expected from the Central Limit Theorem that heat fluxes into patches of a particular size will have a normal distribution. This is confirmed in Figure 9 (b); solid lines are cumulative distributions for simulated heat fluxes over 1 m and 4 m patches and dashed lines are cumulative normal distributions with the same means and standard deviations as the simulated distributions.

Because the blending height is dominated by large patches (Philip 1996) but

the average flux is dominated by small patches, the blending height over a complex snowcover does not provide information on average surface fluxes and neither the tile model nor the extended tile model can be expected to give a good parametrization when driven with temperatures at the blending height. Although fractal objects do not have characteristic length scales and the average patch length for Equation (35) diverges, an average length $\overline{X}$ can be calculated for any finite transect. Comparing results from simulations with regular and complex patterns, an effective patch length such that

$$H_{\text{complex}}(\overline{X}) = H_{\text{regular}}(X_{\text{eff}}) \tag{36}$$

can be defined. For the simulations considered here, it turns out that the effective patch length can be approximated by a linear function $X_{\text{eff}} = 11\overline{X} - 3.2$ for both snow and snow-free patches, as shown by the crosses on Figure 8 (a). The parameters of this approximation will depend on surface and atmospheric characteristics and need to be further investigated, along with characterizations of snowcover geometry and relations to landscape characteristics, to develop a robust parametrization for fluxes over partial snowcovers.

The complex snowcover patterns used here were generated by alternately choosing random snow patch lengths and snow-free patch lengths with the same distribution. Using different distributions for snow and snow-free patches would give patterns with different clustering. Patterns with the same snow patch lengths but different clustering will give different surface fluxes, with average fluxes into snow patches being less for patterns with greater clustering. The degree of clustering, or 'lacunarity', in a pattern can be measured using a gliding-box algorithm introduced by Allain and Cloitre (1991). To extend previous studies of the snowcover geometry, aerial photographs could be analyzed to investigate their lacunarity. This is likely to be strongly influenced by topography and the scale under consideration; a transect crossing snow-free ground on south-facing slopes

and patchy snowcover on north-facing slopes, for example, would have a higher lacunarity than a transect confined to a single slope.

CONCLUSIONS

Results from the simple advection model presented here compare well with temperature profiles and internal boundary layer depths measured over snow patches in fields of varying roughness. The growth of an internal boundary layer can be approximated as a power law of distance downwind from the patch edge, with parameters that depend on surface roughness and atmospheric stability. Because of variations in vertical heat flux with height in the internal boundary layer, standard flux parametrizations that rely on the existence of a constant-flux layer below some reference height cannot be used over snow patches. For isolated snow patches, however, the flux profile can be approximated by an exponential function of height in the internal boundary layer matched to a constant flux above; integrating the flux-gradient relationship using this approximation gives a parametrization for the local surface flux at some point on a snow patch and an approximation for the local temperature profile in the internal boundary layer above the snow. The parametrized temperature profile can be used in an integration of the horizontal advection of heat through the depth of the internal boundary layer at the upwind and downwind edges of a snow patch to estimate the average flux into the patch.

For a partial snowcover of regularly spaced snow patches, surface fluxes can be approximated as power-law functions of patch length. A tile model gives good estimates of average surface fluxes in comparison with the advection model but does not match the fluxes into snow and snow-free patches separately. Applying the exponential approximation to average flux profiles in an extended tile model gives a much better parametrization of local surface fluxes.

Complex patterns of snowcover along transects can be generated by sampling snow and snow-free patch lengths from statistical distributions based on measurements of snowcover geometry. Simulations over complex snowcover patterns give fluxes with a normal distribution for patches of a particular size; the standard deviation and average flux decrease with increasing patch length, and the average can be approximated as a power law with the same exponent as for regular snowcover patterns. It appears that fluxes into snow and snow-free ground for complex patterns can be approximated by those for a regular pattern with an effective patch length that is a linear function of the average length for the complex pattern.

Surface temperatures for snow and snow-free ground were specified as model parameters here. In reality, surface temperatures are determined by the energy balance of the surface and influenced by heterogeneities in characteristics such as the albedo and wetness of the surface. Parametrizations for the full energy balance over partial snowcovers will be considered in future work.

ACKNOWLEDGEMENTS

This work was supported by NERC Advanced Research Fellowship NER/J/S/2001/00812 and Standard Grant NER/A/S/2001/01089. Helpful comments from two anonymous reviewers are acknowledged.

REFERENCES

Abramowitz M, Stegun LA. 1976. Handbook of mathematical functions. Dover, New York, 1046pp.

Allain C, Cloitre M. 1991. Characterizing the lacunarity of random and deterministic fractal sets. *Physical Review A*, **44**: 3552–3558.

Avissar R, Pielke R. 1989. A parametrization of heterogeneous land surfaces for atmospheric numerical models and its impact on regional meteorology. *Monthly Weather Review*, **117**: 2113–2136.

Brutsaert W. 1982. Evaporation into the atmosphere. D. Reidel, Dordrecht, Holland, 299pp.

Cherkauer KA, Lettenmaier DP. 2003. Simulation of spatial variability in snow and frozen soil. *Journal of Geophysical Research*, **108**: art. no. 8858.

Essery RLH. 1997. Modelling fluxes of momentum, sensible heat and latent heat over heterogeneous snowcover. *Quarterly Journal of the Royal Meteorological Society*, **123**: 1867–1883.

Garratt JR. 1992. The atmospheric boundary layer. Cambridge University Press, 316pp.

Granger RJ, Pomeroy JW, Parvianen J. 2002. Boundary layer integration approach to advection of sensible heat to a patchy snowcover. *Hydrological Processes*, **16**: 3559–3569.

Granger RJ, Pomeroy JW, Essery RLH. 2005. Boundary layer growth over snow and soil patches: Field observations. Submitted to *Hydrological Processes*, this issue.

Takahara H, Higuchi K. 1985. Thermal modification of air moving over melting snow surfaces. *Annals of Glaciology*, **6**: 235–237.

Liston GE. 1995. Local advection of momentum, heat and moisture during the melt of patchy snow covers. *Journal of Applied Meteorology*, **34**: 1705–1715.

Mahrt L. 2000. Surface heterogeneity and vertical structure of the boundary layer. *Boundary-Layer Meteorology*, **96**: 33–62.

Marsh P, Pomeroy JW. 1996. Meltwater fluxes at an Arctic forest-tundra site. *Hydrological Processes*, **10**: 1383–1400.

Marsh P, Pomeroy JW, Neumann N. 1997. Sensible heat flux and local advection over a heterogeneous landscape at an Arctic tundra site during snowmelt. *Annals of Glaciology*, **25**: 132–135.

Neumann N, Marsh P. 1998. Local advection of sensible heat in the snowmelt of arctic tundra. *Hydrological Processes*, **12**: 1547–1560.

Philip JR. 1996. One-dimensional checkerboards and blending heights. *Boundary-Layer Meteorology*, **77**: 135–151.

Pohl S, Marsh P. 2005. Small-scale modelling of spatially variable snowmelt in an arctic catchment *Hydrological Processes*, in press.

Rao KS, Wyngaard JC, Coté OR. 1974. Local advection of momentum, heat and moisture in micrometeorology. *Boundary-Layer Meteorology*, **7**: 331–348.

Schmid HP. 1997. Experimental design for flux measurements: matching scales of observations and fluxes. *Agricultural and Forest Meteorology*, **87**, 179–200.

Segal M, Garratt JR, Pielke RA, Ye Z. 1991. Scaling and numerical model evaluation of snow-cover effects on the generation and modification of daytime mesoscale circulations. *Journal of the Atmospheric Sciences*, **48**: 1024–1042.

Shook K, Gray DM, Pomeroy JW. 1993. Temporal variation in snowcover area during melt in prairie and alpine environments. *Nordic Hydrology*, **24**: 183–198.

Shook K, Gray DM. 1997. Synthesizing shallow seasonal snow covers. *Water Resources Research*, **33**: 419–426.

Taylor CM, Harding RJ, Pielke RA, Vidale PL, Walko RL, Pomeroy JW. 1998. Snow breezes in the boreal forest. *Journal of Geophysical Research*, **103**: 23087–23101.

Weisman RN. 1977. Snowmelt: a two-dimensional turbulent diffusion model. *Water Resources Research*, **13**: 337–342.

Wood N, Mason P. 1991. The influence of static stability on the effective roughness lengths for momentum and heat transfer. *Quarterly Journal of the Royal Meteorological Society*, **117**: 1025–1056.

FIGURE CAPTIONS

Figure 1. Temperature profiles measured over snow-free ground ($\diamond$) and 2.5 m downwind from the edge of a snow patch (+), compared with model results over snow-free ground (- - -) and snow (——).

Figure 2. IBL heights from simulations (lines) and measured temperature profiles grouped according to upwind surface roughness in 0.002 - 0.005 m (+) and 0.08 - 0.12 m ($\diamond$) classes.

Figure 3. Exponent b (——) and coefficient c (- - -) obtained by fitting Equation (10) to simulated temperature profiles for variations in (a) upwind surface roughness, (b) windspeed at 2 m, (c) surface temperature difference and (d) upwind surface sensible heat flux. The values marked by crosses for b and diamonds for c on (a) were obtained by fitting to measured temperature profiles.

Figure 4. (a) Heat flux profile with height 10 m downwind from the edge of a snow patch. (b) Temperature profile with height 10 m downwind from the edge of a snow patch. (c) Surface heat flux at distance x from the edge of a snow patch. (d) Average heat flux into a snow patch of length X. Solid lines are from simulations and dashed lines are from parametrizations. Crosses in (a) and (b) show a constant-flux layer and the corresponding temperature profile.

Figure 5. Simulated surface heat fluxes for 50% snowcover in patches of length 5 m (- - -) and 10 m (——).

Figure 6. Coefficient d and exponent n in Equation (23) obtained by fitting to simulations with 10 m snow patches, varying snow-free fetches and $z_0 = 0.001$ m (——) or 0.002 m (- - -).

Figure 7. Advection efficiency as a function of snowcover fraction estimated from measurements over melting tundra snowcovers in 1993 ($\diamond$) and 1996 (+) and from simulations with domain sizes of 20 m (——) and 200 m (- - -).

Figure 8. Surface heat fluxes for snow and snow-free ground, and average fluxes,

for (a) varying snow patch sizes with 50% snowcover and (b) varying snowcover in a 20 m domain. Results are shown from the advection model (——), a tile model (···) and an extended tile model (- - -). For simulations with complex snowcover patterns, fluxes (+) are plotted against an effective patch size $X_{\text{eff}} = 11\overline{X} - 3.2$ in (a).

Figure 9. (a) Average heat fluxes into snow patches (◇) from simulations, with vertical bars extending to plus and minus one standard deviation. The solid line is a power law and the dashed lines are logarithmic fits to the standard deviation. (b) Cumulative distributions of average fluxes into 1 m and 4 m snow patches (——), compared with cumulative normal distributions (- - -).

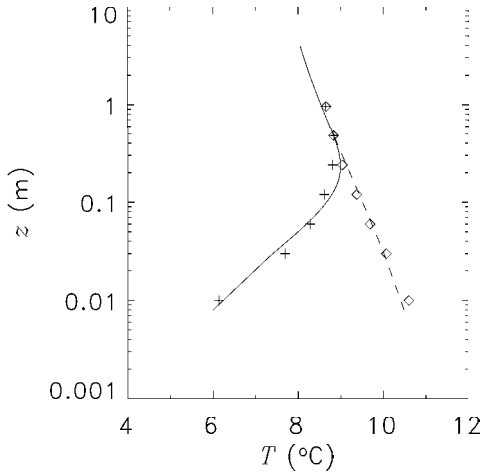

Figure 1.

Temperature profiles measured over snow-free ground ($\diamond$) and 2.5 m downwind from the edge of a snow patch (+), compared with model results over snow-free ground (- - -) and snow (——).

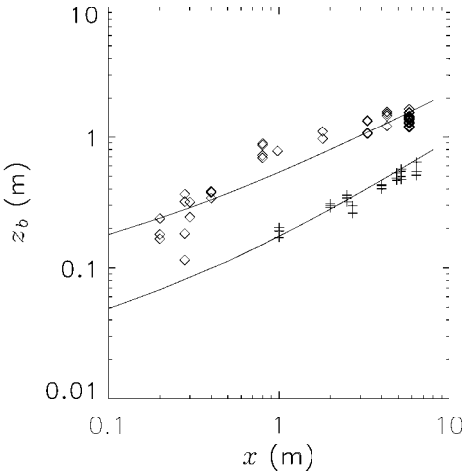

Figure 2.

IBL heights from simulations (lines) and measured temperature profiles grouped according to upwind surface roughness in 0.002 - 0.005 m (+) and 0.08 - 0.12 m ($\diamond$) classes.

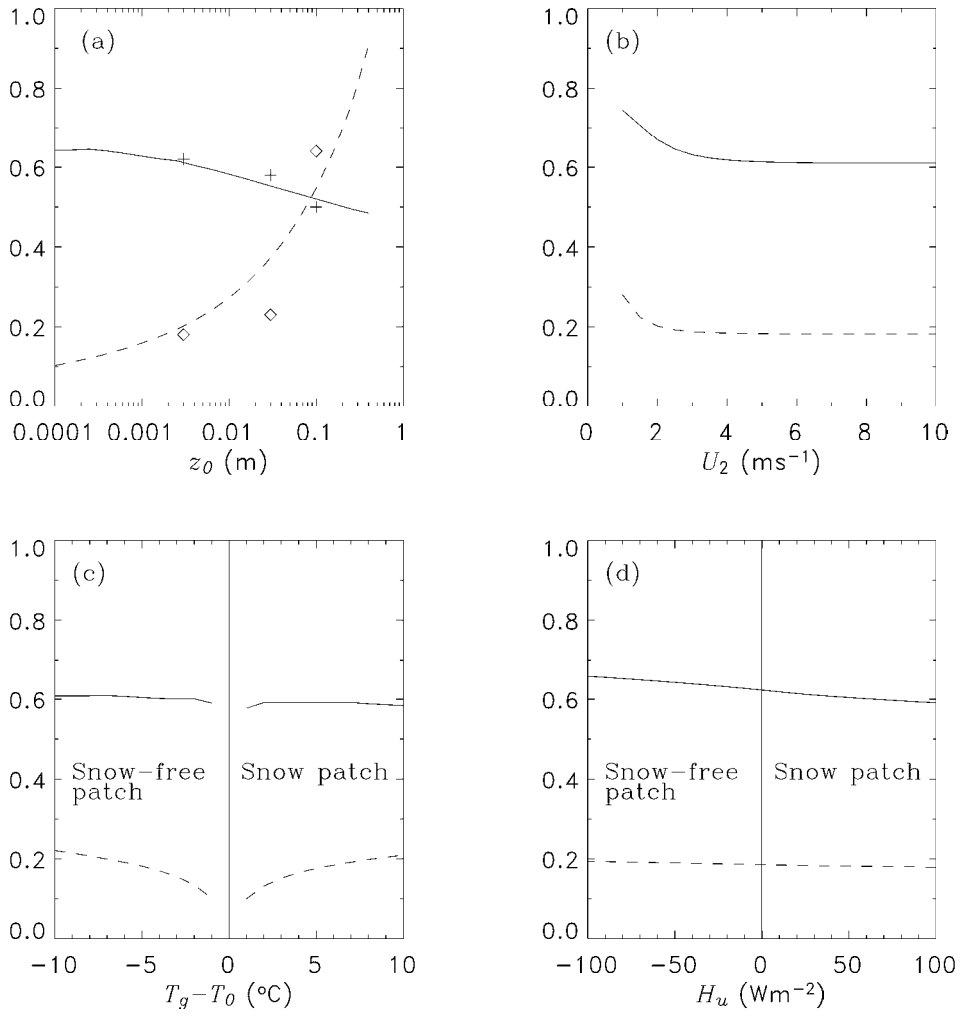

Figure 3.

Exponent b (——) and coefficient c (- - -) obtained by fitting Equation (10) to simulated temperature profiles for variations in (a) upwind surface roughness, (b) windspeed at 2 m, (c) surface temperature difference and (d) upwind surface sensible heat flux. The values marked by crosses for b and diamonds for c on (a) were obtained by fitting to measured temperature profiles.

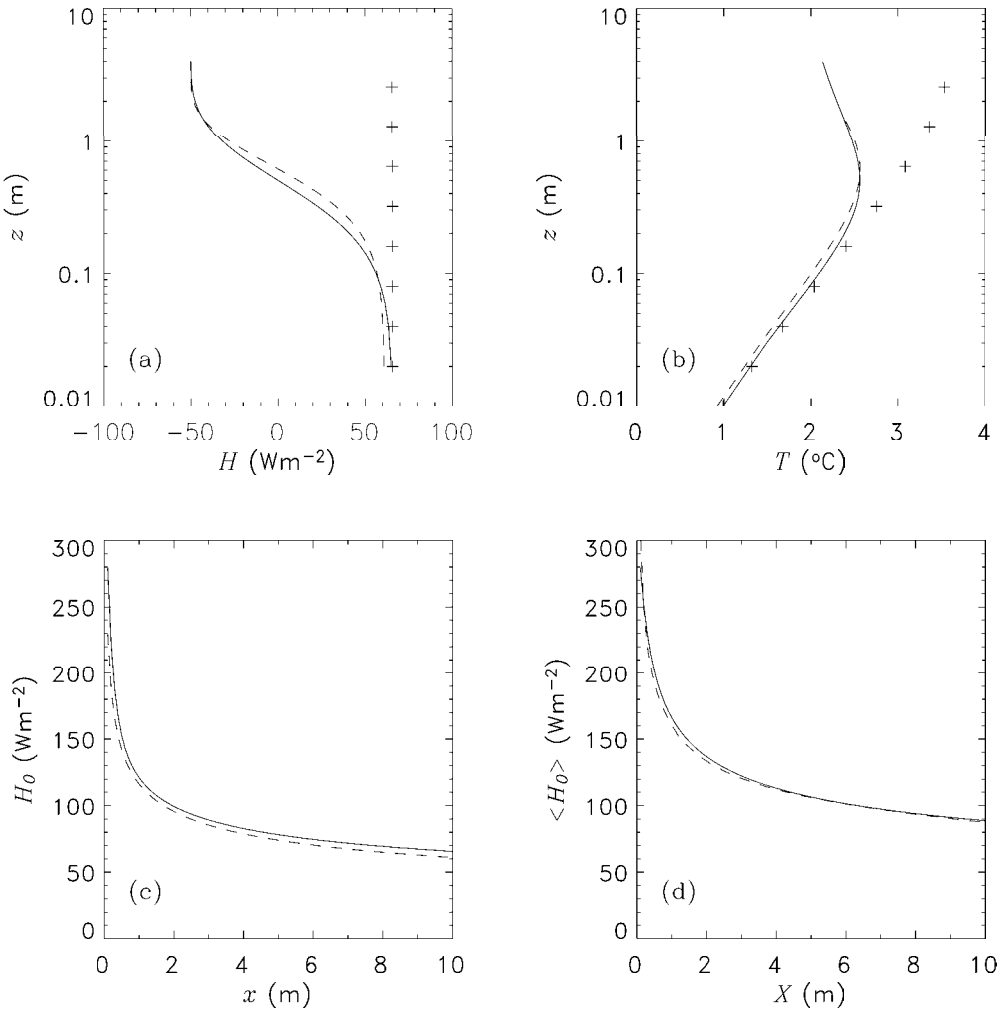

Figure 4.

(a) Heat flux profile with height 10 m downwind from the edge of a snow patch. (b) Temperature profile with height 10 m downwind from the edge of a snow patch. (c) Surface heat flux at distance x from the edge of a snow patch. (d) Average heat flux into a snow patch of length X. Solid lines are from simulations and dashed lines are from parametrizations. Crosses in (a) and (b) show a constant-flux layer and the corresponding temperature profile.

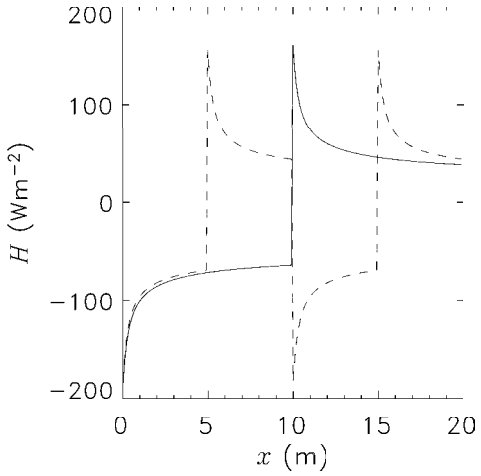

Figure 5.

Simulated surface heat fluxes for 50% snowcover in patches of length 5 m (- - -) and 10 m (——).

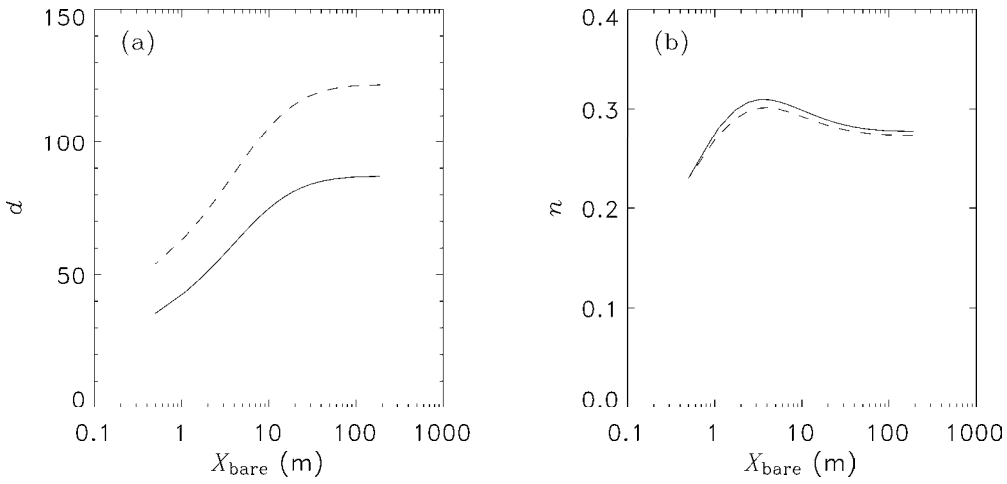

Figure 6.

Coefficient d and exponent n in Equation (23) obtained by fitting to simulations with 10 m snow patches, varying snow-free fetches and $z_0 = 0.001$ m (——) or 0.002 m (- - -).

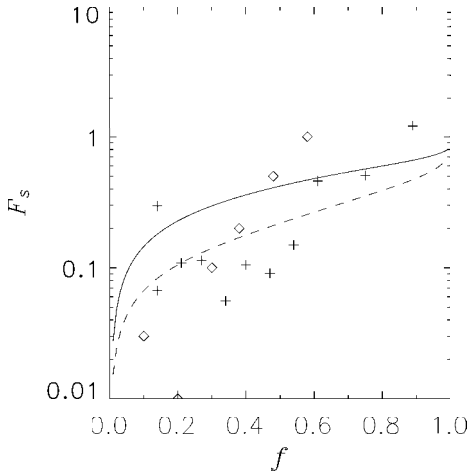

Figure 7.

Advection efficiency as a function of snowcover fraction estimated from measurements over melting tundra snowcovers in 1993 ($\diamond$) and 1996 (+) and from simulations with domain sizes of 20 m (——) and 200 m (- - -).

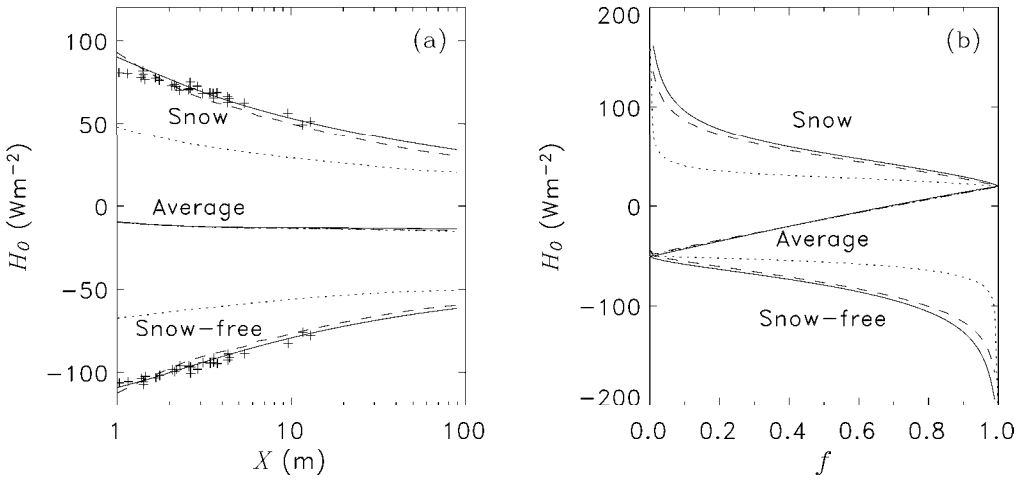

Figure 8.

Surface heat fluxes for snow and snow-free ground, and average fluxes, for (a) varying snow patch sizes with 50% snowcover and (b) varying snowcover in a 20 m domain. Results are shown from the advection model (——), a tile model ($\cdots$) and an extended tile model (- - -). For simulations with complex snowcover patterns, fluxes (+) are plotted against an effective patch size $X_{\text{eff}} = 11\overline{X} - 3.2$ in (a).

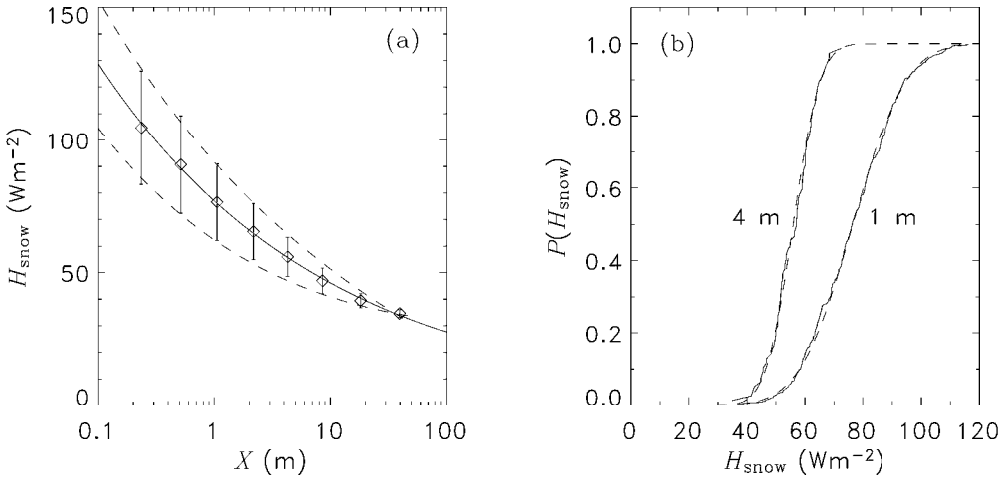

Figure 9.

(a) Average heat fluxes into snow patches ($\diamond$) from simulations, with vertical bars extending to plus and minus one standard deviation. The solid line is a power law and the dashed lines are logarithmic fits to the standard deviation. (b) Cumulative distributions of average fluxes into 1 m and 4 m snow patches (——), compared with cumulative normal distributions (- - -).